Journal of Biomolecular NMR, **12:** 509–521, 1998.
KLUWER/ESCOM

Local mobility of ^{15}N labeled biomolecules characterized through cross-correlation rates: Applications to paramagnetic proteins*

Isabella C. Felli[a], Hervé Desvaux[b] and Geoffrey Bodenhausen[c,**]
[a]*Department of Chemistry, University of Florence, Via Gino Capponi 7, I-50121 Florence, Italy;* [b]*Service de Chimie Moléculaire, Commissariat à l'Energie Atomique, Saclay, F-91191 Gif-sur-Yvette, France;* [c]*Département de Chimie, Ecole Normale Supérieure, 24 rue Lhomond, F-75231 Paris cedex 05, France*

Received 28 February 1998; Accepted 3 July 1998

Key words: cross-correlation, protein dynamics, spin diffusion

Abstract

The mobility of ^{15}N labeled proteins can be characterized by measuring the cross-correlation rates $\delta^{N,NI}$ that govern the conversion of Zeeman order N_z of an amide ^{15}N nucleus into longitudinal two-spin order $2N_zI_z$ involving the amide ^{15}N and ^{1}H nuclei. This represents an alternative to the measurement of ^{15}N self-relaxation rates $1/T_1$ and $1/T_2$ or $1/T_{1\rho}$. The rate of interconversion between N_z and $2N_zI_z$ is due to cross-correlation between fluctuations of different interactions and is not affected by a variety of relaxation mechanisms that contribute to the self-relaxation rates $1/T_1$, $1/T_2$ and $1/T_{1\rho}$. Spin diffusion among protons, which affects the measurements, can be quenched by various means that are evaluated by experiments and simulations. By applying an off-resonance radio-frequency (RF) field in the vicinity of the nitrogen resonance, the spectral density function $J(\omega)$ can be determined at the frequency origin and at the nitrogen Larmor frequency. The methods are applied to the paramagnetic High-Potential Iron-Sulfur Protein iso I (HiPIP I) from *E. halophila* in its reduced state.

Introduction

The longitudinal and transverse self-relaxation $\rho^N = 1/T_1$, $1/T_2$ and $1/T_{1\rho}$ of ^{15}N nuclei and the cross-correlation (Overhauser) rates σ^{NI} involving neighbouring protons I_l can yield valuable insight into internal dynamics of macromolecules (Wagner, 1993; Palmer et al., 1996). The interpretation of these rates is straightforward if a number of assumptions are fulfilled (Kay et al., 1989): (i) if the relaxation within the N-I spin pairs is caused predominantly by N-I dipole-dipole and N-spin CSA interactions; (ii) if the N-I spin pairs are reasonably isolated from their environment, so that interactions between neighbouring and remote protons I_l and I_k need not be taken into account; (iii) if the local and overall dynamics can be described in terms of two correlation times (Lipari and Szabo, 1982). Under these assumptions, one can determine a local order parameter S_i^2 and a local correlation time τ_{ci}. It is also possible to map the spectral densities without any assumptions regarding the motional model (Peng and Wagner, 1992). However, the accuracy of the measurement of self-relaxation rates is usually not sufficient to allow a precise evaluation of the spectral densities (Peng and Wagner, 1995), unless it is assumed that the spectral density is uniform over a limited range, so that $J(\omega_I + \omega_N) = J(\omega_I) = J(\omega_I - \omega_N)$, where ω_I and ω_N are the Larmor frequencies. With this assumption, it is sufficient to measure three independent relaxation rates at a given static magnetic field strength, since the spectral density function can be characterized by only three values $J(0)$, $J(\omega_N)$, and $J(\omega_I)$ (Kay et al., 1992; Palmer et al., 1992; Farrow et al., 1994; Dayie and Wagner, 1996; Lefèvre et al., 1996).

In diamagnetic proteins, the contributions from the N-I dipole-dipole interaction and the CSA of the N spin are likely to be predominant, so that other

*This work was carried out at the Center for Interdisciplinary Magnetic Resonance, National High Magnetic Field Laboratory, 1800 East Paul Dirac Drive, Tallahassee, FL 32310, U.S.A.
**To whom correspondence should be addressed.

mechanisms may be neglected. However, even in N-H subsystems in amides, the magnitude of the chemical shift anisotropy may vary from one residue to another, and it may not be satisfactory to assume an average CSA of 160 ppm (Tjandra et al., 1996a). Furthermore, chemical exchange in N-H groups may contribute to the apparent transverse relaxation rates (Palmer et al., 1996). In paramagnetic proteins, unpaired electrons lead not only to dipolar and contact interactions, but also to dipolar interactions between the Curie spin (average magnetic moment associated with the electrons) and the nuclear spins, which lead to an enhancement of the self-relaxation rates of the N spin (Solomon, 1955; Guéron, 1975; Vasavada and Nageshwara Rao, 1989; Banci et al., 1991; Bertini et al., 1996c).

Cross-correlations between fluctuations of different interactions can provide structural and dynamic information, provided satisfactory protocols can be developed for their accurate measurement (Tjandra et al., 1996a; Reif et al., 1997; Pervushin et al., 1997). We shall focus attention on the cross-correlation rate $\delta^{N,NI}$, i.e. the rate of conversion of Zeeman order N_z into longitudinal two spin order $2N_zI_z$. In diamagnetic systems, such a conversion can only occur when there is a correlation between the fluctuations of the ^{15}N CSA and the *N-I* dipole-dipole interactions. In paramagnetic systems, there are three relaxation mechanisms due to unpaired electrons that can contribute to the self-relaxation rates of the nuclei, but only the Curie mechanism (dipolar interaction with the average electronic magnetic moment) can contribute to the cross-correlation rate $\delta^{N,NI}$. Chemical or conformational exchange processes are not expected to contribute significantly to this rate. In the absence of an RF field, the rate $\delta^{N,NI}$ depends only on the spectral density $J(\omega_N)$. When the ^{15}N magnetization is locked along an effective field tilted by an angle θ_N with respect to the static magnetic field, the cross-correlation rate $\delta^{N,NI}$ also depends on $J(0)$. Comparison of the rates $\delta^{N,NI}$ measured with (at least) two different angles θ_N allows one to separate the contributions of $J(0)$ and $J(\omega_N)$.

We shall give expressions for cross-correlation rates $\delta^{N,NI}$ when the I and/or N magnetization components are locked along tilted effective fields. Effects of spin-diffusion due to cross-relaxation rates $\sigma^{l,k}$ between neighbouring and remote protons I_l and I_k will be discussed, and different schemes for quenching spin diffusion will be compared by simulation and experiment. The methods have been applied to the High-Potential Iron-Sulfur Protein iso I (HiPIP I) obtained from the photosynthetic bacterium *E. halophila*. This is a protein with 73 amino acids containing an Fe_4S_4 cluster. Formally, two of the iron atoms in the reduced state should have an oxidation state +2 and the other two an oxidation state +3. It appears however that all four iron atoms are equivalent with a non-magnetic ground state (S = 0) (Dickson et al., 1974). Since the excited states are partly populated at room temperature, they have significant effects on nuclear relaxation (Banci et al., 1994; Bertini et al., 1996a, b).

Theory

We shall consider a sub-system comprising a spin N, its nearest neighbour proton I_l, and, for computational convenience, no more than twelve remote protons I_k(k = 1 ... 12). We consider the terms N_z, I_{lz}, I_{kz}, $2N_zI_{lz}$ and $2N_zI_{kz}$. These components may be locked along (possibly tilted) effective fields. A system of coupled differential equations is defined in analogy to the Solomon equations, with a matrix **R** that contains all self- and cross-relaxation rates. If there are 12 remote protons, we have a system of 27 coupled equations. An RF field with a carrier frequency ω_N^{rf} and an amplitude ω_{1N} is applied in the vicinity of the Larmor frequency ω_N. This gives rise to a tilted effective field with an amplitude $\omega_N^{eff} = \sqrt{(\omega_{1N})^2 + (\omega_N - \omega_N^{rf})^2}$ and a tilt angle θ_N with respect to the static magnetic field:

$$\theta_N = \arctan\left(\frac{\omega_{1N}}{\omega_N - \omega_N^{rf}}\right) \tag{1}$$

Another RF field with a carrier frequency ω_I^{rf} is applied in the vicinity of the proton Larmor frequency ω_I of the nearest neighbour proton I_l, leading to an effective field with an amplitude ω_I^{eff} and a tilt angle θ_I. Analogous expressions can be written for the remote spins I_k. For simplicity, we shall assume that the transverse component ω_{1I} is much larger than the range of offsets of all spins I_l and I_k, so that all tilt angles θ_l and θ_k may be assumed to be equal for $k = 1 \ldots 12$. These angles will be denoted by the common symbol θ_I. The time-dependence of the density operator σ can be calculated as a function of the mixing time τ_m by diagonalisation:

$$\begin{aligned}\sigma(\tau_m) &= \exp(-\mathbf{R}\tau_m)\cdot\sigma(0)\\ &= \mathbf{V}\cdot\exp(-\mathbf{\Lambda}\tau_m)\cdot\mathbf{V}^{-1}\cdot\sigma(0)\end{aligned} \tag{2}$$

where the eigenvalues of $\mathbf{\Lambda}$ and the elements of **V** depend on the tilt angles θ_N and θ_I. For proton systems,

the relaxation rates in the presence of tilted effective fields have been given elsewhere (Desvaux, 1997). The Hamiltonian in the laboratory frame is:

$$\begin{aligned} H(t) = {} & \omega_N N_z + \omega_I I_{lz} + \Sigma_k \omega_I I_{kz} \\ & + 2\omega_{1N} \cos(\omega_N^{rf} t) N_x \\ & + 2\omega_{1I} \cos(\omega_I^{rf} t)[I_{lx} + \Sigma_k I_{kx}] \\ & + H_1(t) \end{aligned} \quad (3)$$

where $H_1(t)$ contains time-dependent dipolar and CSA interactions which are responsible for relaxation. The cross-relaxation rate (NOE) between neighbour and remote proton components I_{lz} and I_{kz} locked along the same tilted effective field is determined by the spectral density $J_{lk}(\omega)$

$$\begin{aligned} \sigma_{Ik}^{Ik} = {} & \left(\sin^2\theta_I - \frac{1}{3}\right) J_{Ik}(0) + \sin^2\theta_I J_{Ik}(\omega_I) \\ & + 2\cos^2\theta_I J_{Ik}(2\omega_I) \end{aligned} \quad (4)$$

where we have used the normalization of Desvaux, 1997, for the spectral density functions. A similar expression applies for a pair of remote protons I_k and $I_{k'}$. The superscripts on the rate σ indicate the density operator components ('reservoirs') that are coupled together, while the subscripts refer to the interactions that are responsible for their coupling. This notation may appear redundant in simple cases such as Equation 4, but will be useful below. When two components N_z and I_z are locked along their respective tilted fields, their cross-relaxation rate (heteronuclear NOE) is:

$$\begin{aligned} \sigma_{NI}^{NI} = {} & \cos\theta_I \cos\theta_N \left[-\frac{1}{3} J_{NI}(\omega_I - \omega_N)\right. \\ & \left. + 2J_{NI}(\omega_I + \omega_N)\right] \end{aligned} \quad (5)$$

The rate of interconversion between N_z and $2N_z I_z$ arising from cross-correlation between the CSA of spin N and the dipole-dipole interaction N-I is:

$$\begin{aligned} \delta_{N,NI}^{N,NI} = {} & -\cos\theta_I \left[\frac{8}{3}\sin^2\theta_N J_{N,NI}(0)\right. \\ & \left. + 2(1+\cos^2\theta_N) J_{N,NI}(\omega_N)\right] \end{aligned} \quad (6)$$

where $J_{N,NI}$ is the relevant spectral density function. Note that in the absence of an RF field applied in the vicinity of the ^{15}N resonance (i.e., when $\theta_N = 0$), this expression reduces to $\delta_{N,NI}^{N,NI} = -4\cos\theta_I J_{N,NI}(\omega_N)$, which is small in macromolecules. In the slow motion limit, the cross-correlation rate $\delta_{N,NI}^{N,NI}$ greatly increases if one applies an RF field in the vicinity of the ^{15}N resonance so that $\theta_N \neq 0$. If the internuclear distance and the angle subtended between the principal axis of the CSA tensor and the NH bond vector are constant, the two spectral density functions J_{NI} and $J_{N,NI}$ are proportional to each other. The contribution to the self-relaxation rate of $2N_z I_z$ that arises from the dipolar interaction between N and I is:

$$\begin{aligned} \rho_{NI}^{NI} = {} & \frac{2}{3}\left[\sin^2\theta_I \cos^2\theta_N + \sin^2\theta_N \sin^2\theta_I\right] \\ & J_{NI}(0) \\ & + \frac{1}{2}\left[(1+\cos^2\theta_N)\cos^2\theta_I + \sin^2\theta_N\right. \\ & \left. \sin^2\theta_I\right] J_{NI}(\omega_N) \\ & + \frac{1}{12}\left[(1+\cos^2\theta_N)\sin^2\theta_I + \right. \\ & \left. \sin^2\theta_N(1+\cos^2\theta_I)\right] J_{NI}(\omega_I - \omega_N) \\ & + \frac{1}{2}\left[(1+\cos^2\theta_I)\cos^2\theta_N + \right. \\ & \left. \sin^2\theta_N \sin^2\theta_I\right] J_{NI}(\omega_I) \\ & + \frac{1}{2}\left[(1+\cos^2\theta_N)\sin^2\theta_I + \sin^2\theta_N(1+\right. \\ & \left. \cos^2\theta_I)\right] J_{NI}(\omega_I + \omega_N) \end{aligned} \quad (7)$$

Except for contributions from fast exchange processes (Akke and Palmer, 1996; Zinn-Justin et al., 1997), all other self-relaxation rates result from a weighted average of longitudinal and transverse rates corresponding to $\theta_i = 0°$ and $90°$:

$$\rho(\theta_i) = \rho(\theta = 0°)\cos^2\theta_i + \rho(\theta = 90°)\sin^2\theta_i \quad (8)$$

where i may stand for one of the spins N, I_l or I_k. The presence of a paramagnetic center leads to an enhancement of all self-relaxation rates. These contributions can be evaluated by combining Equation 8 with expressions for relaxation rates $1/T_1$ and $1/T_2$ arising from dipolar and contact terms between nuclei and electrons (Solomon, 1955; Guéron, 1975; Vasanada and Nageswara Rao, 1989; Banci et al., 1991; Bertini et al., 1996c). Dipolar interactions involving a paramagnetic center may also induce cross-correlation effects (Bertini et al., 1993; Werbelow and Thévand, 1993; Mäler et al., 1996). Cross-correlation between the dipole-dipole interactions N-S and N-I may contribute to the rate of interconversion between N_z and $2N_z I_z$:

$$\begin{aligned} \delta_{NS,NI}^{N,NI} = {} & \cos\theta_I \left[\frac{8}{3}\sin^2\theta_N J_{NS,NI}(0)\right. \\ & \left. + 2(1+\cos^2\theta_N) J_{NS,NI}(\omega_N)\right] \end{aligned} \quad (9)$$

Again, the superscript indicates the reservoirs that are interconnected, while subscripts indicate the interactions that are responsible for the flow of order from one reservoir to another. A comma is used when more than two spins are involved. Note that $J_{NS,NI}(\omega)$ is usually

not proportional to J_{NI} (ω), since it represents the Fourier transformation of the cross-correlation function of the *N-S* and *N-I* vectors, which is not only affected by the motion of the *N-I* vector, but also by fluctuations of the *N-S* distance, by the relative motion of these two vectors, and by the *S* spin dynamics. Cross-correlation between the dipolar *N-I* and the *N-S* interactions involves the *average* Curie magnetic moment <*S*> of the electron. Rapidly fluctuating contributions average out, while the contact interaction cannot contribute because it is characterized by a tensor of a different rank.

Cross-correlation between the fluctuations of chemical shifts and J coupling constants can contribute to the rate $\delta^{N,NI}$ (Brüschweiler and Ernst, 1991). In practice, these contributions are believed to be very small in proteins.

To summarize, the flow between the Zeeman reservoir N_z and the two-spin order $2N_zI_z$ is determined by two contributions:

$$\delta^{N,NI} = \delta^{N,NI}_{N,NI} + \delta^{N,NI}_{NS,NI} \tag{10}$$

the first (diamagnetic) term is due to cross-correlation beween the fluctuations of the CSA of the *N* spin and the *N-I* dipole-dipole interaction, while the second (paramagnetic) term is due to cross-correlation between the *N-S* and *N-I* dipole-dipole interactions. In the experimental cases discussed below, the paramagnetic contribution $\delta^{N,NI}_{NS,NI}$ is much smaller than the diamagnetic contribution $\delta^{N,NI}_{N,NI}$ for all ^{15}N nuclei that are not too close to the Fe_4S_4 center which is only weakly paramagnetic. We shall therefore disregard the paramagnetic term in Equation 10. However, paramagnetic contributions to the self-relaxation rates of Equation 8 will be taken into consideration.

Ratios of build-up initial rates

If we recall that J_{NI} and $J_{N,NI}$ are usually considered to be proportional to each other, the measurement of the cross-correlation rate $\delta^{N,NI}_{N,NI}$ of Equation 6 with two different tilt angles θ_N and θ'_N, and of the cross-relaxation rate (NOE) σ^{NI}_{NI} of Equation 5 with $\theta_N = 0$ can provide three independent measurements that suffice to determine the spectral density function J_{NI} at the three frequencies 0, ω_N, and ω_I. The cross-correlation rate can be obtained from the initial slope $\kappa^{N,NI}$ of the build-up curve of the conversion of N_z into $2N_zI_z$:

$$\kappa^{N,NI} = \lim_{\tau_m \to 0}\left[\frac{d}{d\tau_m} a^{N,NI}(\tau_m)\right]$$

$$= -\delta^{N,NI} N_z(0) \tag{11}$$

where τ_m is the mixing time, $a^{N,NI}(\tau_m)$ the amplitude of the corresponding cross peak in a two-dimensional spectrum (see below), and $N_z(0)$ the expectation value of the ^{15}N Zeeman term at the beginning of the mixing time. The measurement of the initial magnetization $N_z(0)$ requires a complementary experiment, in analogy to cross-relaxation measurements in C_α-CO systems (Cordier et al., 1996; Zeng et al., 1996). Fortunately, this can be avoided by comparing initial slopes obtained with different tilt angles θ_N. Indeed, the initial slope $\kappa^{N,NI}$ should have the same dependence on θ_N as $\delta^{N,NI}$, since $N_z(0)$ does not depend on θ_N, provided the effective field is rotated adiabatically (see below). When the initial slope $\kappa^{N,NI}$ is measured with two different tilt angles, i.e. with $\theta_N = 0$ and $\theta_N \neq 0$, one obtains a system of two equations derived from Equations 6 and 11 which can be solved to determine the ratio

$$r = \frac{J_{N,NI}(\omega_N)}{J_{N,NI}(0)} = \frac{2\sin^2\theta_N}{3} \frac{\kappa^{N,NI}(\theta_N = 0)}{\kappa^{N,NI}(\theta_N) - \frac{1}{2}(1+\cos^2\theta_N)\kappa^{N,NI}(\theta_N = 0)} \tag{12}$$

This ratio *r* is independent of the initial magnetization $N_z(0)$ and of the tilt angle θ_I of the effective field applied in the vicinity of the protons. *The ratio r provides a valuable measure of local mobility.* Fast motions should cause an increase of $J_{N,NI}(\omega_N)$ and a concomittant decrease of $J_{N,NI}(0)$. Therefore, a large ratio *r* should be indicative of the presence of fast internal motions, while a small ratio *r* should reflect local 'rigidity'. Qualitatively, the ratio *r* can be interpreted in a similar fashion as the ratio T_2/T_1 discussed by Tjandra et al. (1996b) but it has the advantage that no assumptions need to be made about contributions from different mechanisms. Indeed, the ratio *r* of Equation 12 is independent of the N-H distance (which can vary due to hydrogen bonding), independent of the chemical shift anisotropy $\Delta\sigma$, (which may vary from one amino acid to another) (Tjandra et al., 1996a), and is not affected by chemical exchange.

Materials and methods

A sample of ^{15}N labeled HiPIP I was isolated and purified from *E. coli* cultures grown in a minimal M9 medium enriched with $(^{15}NH_4)_2SO_4$ (0.3 g/l). About 10 mg purified protein was exchanged through ultrafiltration (YM3 membranes, Amicon) with 50 mM

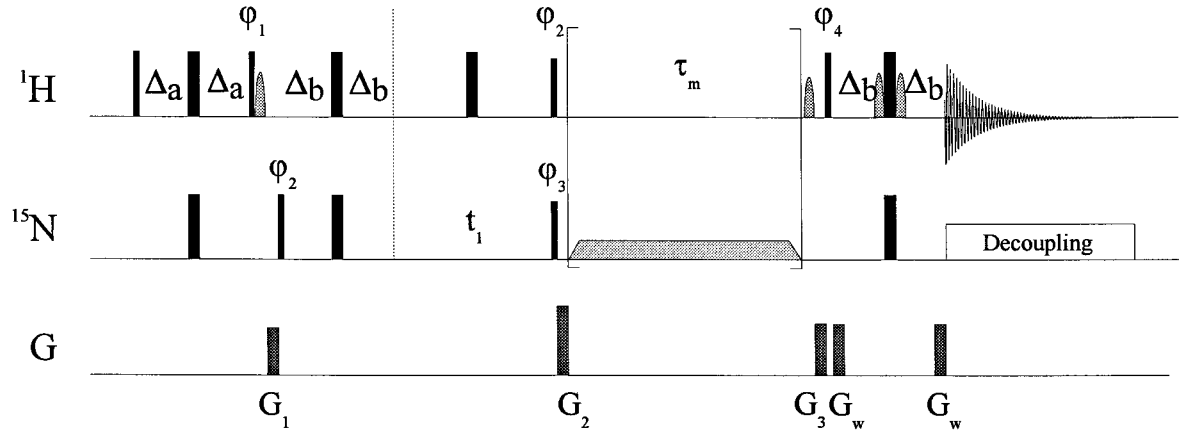

Figure 1. Pulse sequence used to measure the rate of conversion $\delta^{N,NI}$ (cross-correlation rate) of Zeeman order N_z into longitudinal two-spin order $2N_zI_{lz}$. The phase cycle was ϕ_1 = (y,y,−y,−y,y,y,−y,−y), ϕ_2 = (x,−x,x,−x,x,−x,x,−x), ϕ_3 = (y,y,y,y,−y,−y,−y,−y), ϕ_4 = (y,y,y,y,y,y,y,y,), ϕ_{rec} = (x,−x,−x,x,−x,x,x,−x). All other pulses have phase x. The delays Δ_a = 2.5 ms and Δ_b = 2.3 ms were set slightly below $(4\,{}^1J_{NH})^{-1}$. The first selective RF pulse, which is applied to the water resonance, had a 'seduce' shape with a duration of 1.4 ms. The second selective pulse had a Gaussian shape, a nutation angle of 270°, and a duration of 2.2 ms. The last two water suppression pulses had 'seduce' shapes and a duration of 1.27 ms each. The durations and strengths of the field gradient pulses were: G_1(0.8 ms, 8 G/cm), G_2 (3 ms, 25 G/cm), G_3 (0.5 ms, 5 G/cm), G_w (0.5 ms, 8 G/cm). An off-resonance RF field may be applied to the nitrogen-15 spins with an RF amplitude that must be increased and decreased adiabatically.

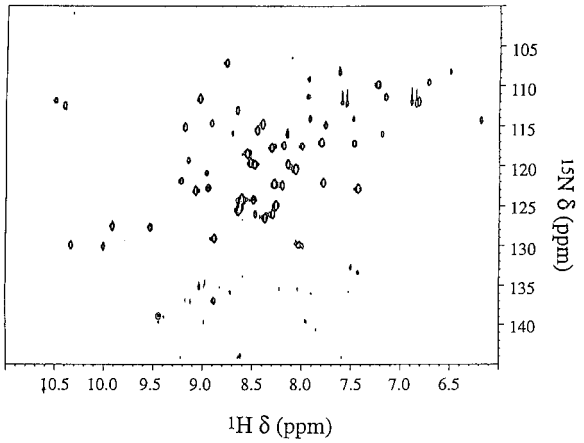

Figure 2. Two-dimensional ^{1}H-^{15}N heteronuclear correlation spectrum of HiPIP I from *E. halophila* recorded at 720 MHz with the sequence of Figure 1 (mixing time τ_m = 70 ms) using off-resonance irradiation in the vicinity of both ^{15}N and ^{1}H resonances ($\theta_N = \theta_I = 35°$). The total experimental time was about 3 h.

potassium phosphate buffer, and the pH was gradually lowered to 5.0. The sample was concentrated to 450 µl and reduced under anaerobic conditions by adding 20 µl of a 0.15 M buffered isoascorbate solution. The final protein concentration was about 2 mM. All spectra were acquired at a temperature of 288 K on a Varian Unity Plus spectrometer at the National High Magnetic Field Laboratory in Tallahassee, Florida, with a static field B_0 = 16.8 T and a proton Larmor frequency of 720 MHz. An inverse triple-channel probe with a self-shielded *z* gradient coil was used. Each two-dimensional spectrum consisted of 4K complex points in t_2 and of 64 increments in t_1, extended by zero-filling to 128 points. The data were weighted with a squared cosine function in both dimensions. The cross peaks were integrated after Fourier transformation. The assignments were taken from the work of Bertini et al. (1994, 1996b).

The basic sequence used to measure the conversion of N_z into $2N_zI_z$ is shown in Figure 1. This is closely related to experiments due to Boyd et al. (1991). We have chosen to monitor the interconversion of N_z into $2N_zI_z$ *after* the evolution time t_1. Only one 180° pulse needs to be applied to the ^{15}N spins after the mixing time τ_m. The off-resonance RF fields are increased and decreased in trapezoidal fashion to allow the magnetization to rotate adiabatically back and forth between the directions of the static and the tilted effective fields (Desvaux et al., 1995). For the ^{15}N spins, the irradiation was applied at one chosen offset, and the dispersion of the tilt angles experienced by various nuclei was taken into consideration during data processing. The phase cycling (see caption) was chosen so that the signals vanish for long mixing times (Sklenar et al., 1987). A hard 90° pulse applied to the protons was followed by a strong dephasing gradient G_2 before the mixing time τ_m to eliminate any unde-

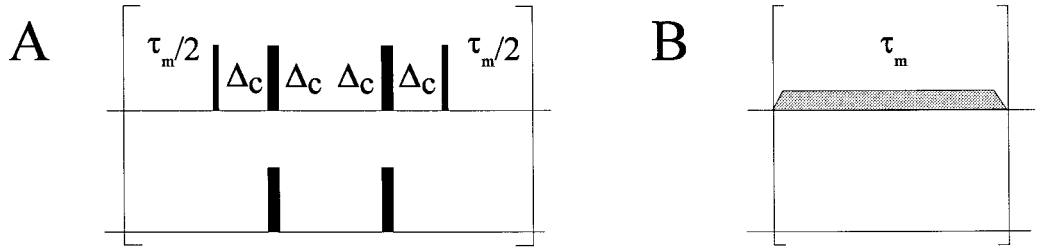

Figure 3. Schemes used to quench spin-diffusion between the protons during the mixing time of the sequence of Figure 1. (A) Sequence that leads to the inversion of all longitudinal terms except N_z and $2N_zI_{1z}$ in the middle of τ_m in analogy to the QUIET method. The delays Δ_c must be $(4\ ^1J_{NH})^{-1} = 2.7$ ms. (B) Off-resonance field applied to the protons so that the effective field subtends an angle $\theta_I = 35°$ with respect to the z axis. The field amplitude must be increased and decreased slowly (typically in 3 ms) so that the magnetization components are rotated adiabatically.

sirable I_z and $2N_zI_z$ terms, so that the signal vanishes for $\tau_m = 0$. Water suppression was obtained by a combination of water flip-back pulses (Grzesiek and Bax, 1993) and the Watergate scheme (Piotto et al., 1992). The latter is implemented during the final delay that is required to refocus $2N_zI_x$ into I_y magnetization. Sign discrimination in the ω_1 dimension is obtained by the States-TPPI method with phase-shifts of the first ^{15}N 90° pulse (Marion et al., 1989).

Build-up curves were recorded with the sequence of Figure 1 with $\theta_N = 0°$ (i.e. without spin-locking field), with $\theta_N = 25°$, and with $\theta_N = 35°$, in the latter case with the RF carrier placed on opposite sides of the resonance frequency. A typical 2D spectrum obtained with $\theta_N = \theta_I = 35°$ is shown in Figure 2. All build-up curves were sampled with 13 to 17 τ_m increments between 20 and 400 ms (and up to 900 ms for $\theta_N = 0°$). The amplitude of the RF field applied near the ^{15}N resonance was 0.92 or 1.2 kHz. In experiments where an RF field was applied near the ^{1}H resonance, its amplitude was 5 kHz. The experimental cross-peak intensities $a^{N,NI}(\tau_m)$ were compared by a least-square fitting procedure using a Levenberg-Marquard algorithm (Press et al., 1992) with a biexponential function with two eigenvalues λ_1 and λ_2, suitable for a system of two coupled differential equations (see below):

$$a^{N,NI}(\tau_m) = A[\exp(-\lambda_1\tau_m) - \exp(-\lambda_2\tau_m)] \quad (13)$$

Numerical simulations have been carried out using a program written in C with parameters corresponding to the experimental study. The distances and angles between the nuclei were derived from the solution structure of HiPIP I as recorded in the Protein Data Bank (Banci et al., 1994, Bertini et al., 1996b). We assumed an isotropic Brownian motion with an overall correlation time $\tau_c = 4$ ns, an ^{15}N CSA tensor with a cylindrical symmetry with $\Delta\sigma = -160$ ppm, and a principal axis assumed to be parallel to the N-H vector. The self-relaxation rates (diagonal elements of the **R** matrix) were estimated from Equations 7 and 8 by summing over the dipolar interactions between all spin pairs within a cluster, considering the contributions of the ^{15}N CSA and the dipolar couplings to the electron spins associated with each of the four iron atoms. We neglected the contact and Curie spin contributions, but not the dipolar contributions of the electron spin to the nuclear relaxation. The spectral density functions of the dipolar electron-nuclear interactions were assumed to be the same for all spin pairs (Bertini et al., 1996b).

To estimate errors of the initial slopes $\kappa^{N,NI}$, random errors generated by a Monte Carlo algorithm were added to simulated build-up curves, and biexponential functions were fitted to the resulting noisy curves. From the best-fitted functions, the initial slopes were derived:

$$\kappa^{N,NI} = \frac{d}{d\tau_m} a^{N,NI}(\tau_m) = A[\lambda_2 - \lambda_1] \quad (14)$$

The associated errors were also determined. Thus, no assumptions need to be made about the independence of the errors of the three parameters A, λ_1 and λ_2.

We have considered various schemes to quench spin diffusion (Figure 3) and checked their efficiency both experimentally and by numerical simulations. To this effect, we have calculated the expected time-dependence of a cross-peak amplitude $a^{N,NI}(\tau_m)$ and then fitted the build-up with Equation 13 to estimate the initial slope $\kappa^{N,NI}$ defined in Equation 14. Since the initial magnetization is not known, Equation 12 is used to determine the ratio r of the spectral densities.

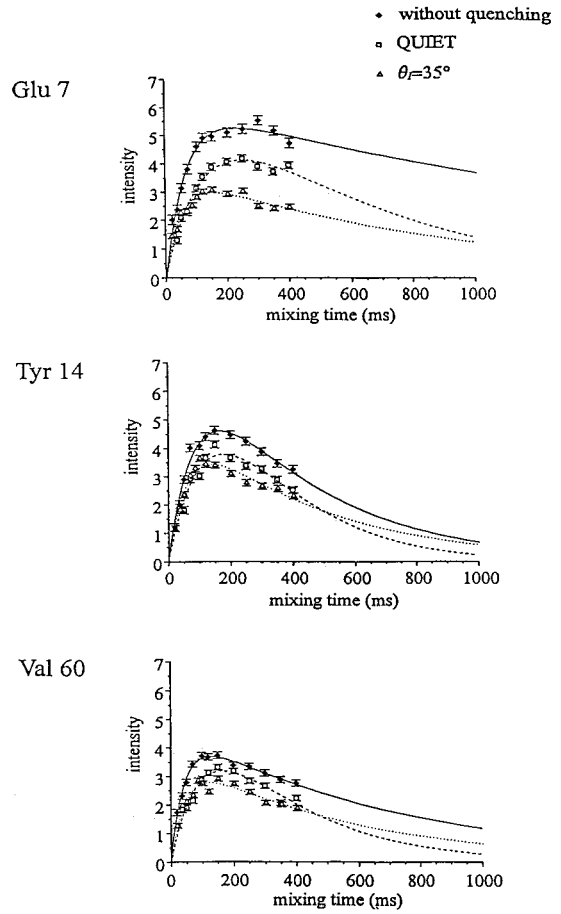

Figure 4. Experimental build-up curves showing the conversion of N_z into $2N_zI_{1z}$ order for three amino-acids in HiPIP I: Glu[7], Tyr[14], Val[60]. The filled diamonds were obtained without quenching spin diffusion in the mixing time, open squares with the QUIET scheme of Figure 3A, and open triangles with off-resonance proton irradiation with a tilt angle $\theta_I = 35°$ (Figure 3B). The continuous curves correspond to best fits to the biexponential function of Equation 13.

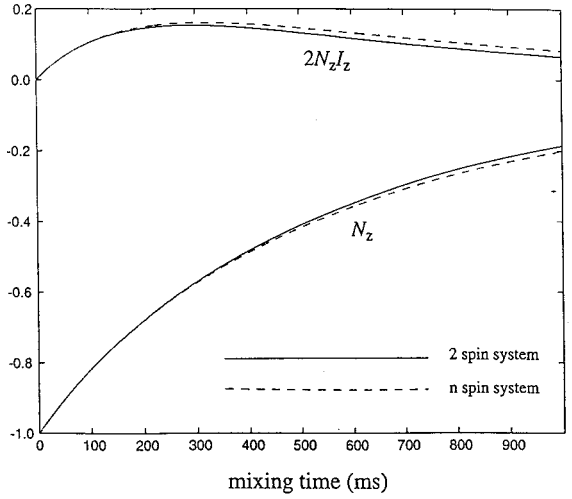

Figure 5. Simulated recovery of inverted Zeeman magnetization $-N_z$ and build-up of $2N_zI_{1z}$ considering either (dashed line) a complete relaxation matrix **R** including 12 remote protons or (solid line) only a simplified two-dimensional relaxation matrix **R** as in Equation 15.

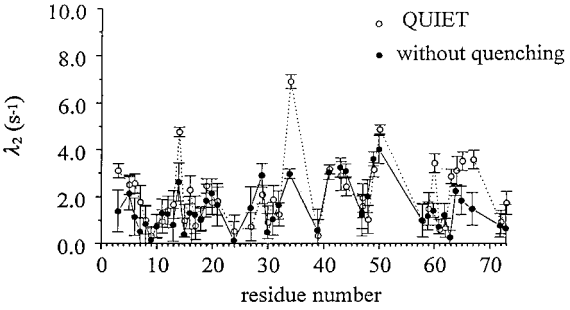

Figure 6. The smallest eigenvalues λ_2 (longest time-constants) obtained by fitting the bi-exponential function of Equation 13 to experimental build-up curves obtained with the basic experiment of Figure 1 (filled circles) and with the QUIET experiment of Figure 3A (open circles) for all observable amino-acid residues in HiPIP I.

Results and discussion

If the N-H system were truly isolated from its environment, the interconversion of N_z and $2N_zI_z$ could be described by reducing the dimensions of the matrix **R** in Equation 2:

$$\frac{d}{dt}\langle 2N_zI_z\rangle(\tau_m) = -\delta^{N,NI}\langle N_z\rangle(\tau_m) - \rho^{NI}\langle 2N_zI_z\rangle(\tau_m) \qquad (15)$$

$$\frac{d}{dt}\langle N_z\rangle(\tau_m) = -\rho^{N}\langle N_z\rangle(\tau_m) - \delta^{NI,N}\langle 2N_zI_z\rangle(\tau_m)$$

It is not necessary to consider the time-dependence of $\langle I_z\rangle$ because the coupling between this reservoir and $\langle N_z\rangle$ through cross-relaxation is much weaker than the coupling between $\langle N_z\rangle$ and $\langle N_zI_z\rangle$ through cross-correlation. In practice however, we cannot disregard the effect of spin diffusion on the time dependence of $2N_zI_z$. Indeed, for a medium-sized protein with $\tau_c = 4$ ns at 16.8 T (720 MHz), the rate $\delta^{N,NI}$ is comparable to the homonuclear cross-relaxation rate σ^{kl} between two protons I_k and I_l separated by 230 pm ($\delta^{N,NI} = 1.52\ s^{-1}$ and $\sigma^{kl} = 1.51\ s^{-1}$). An accurate description requires a sum of m exponentials, in a manner that is reminiscent of NOESY build-up curves (Boelens et al., 1988; Borgias et al., 1990; Malliavin et al., 1992). Like in NOESY, the rate $\delta^{N,NI}$ can in principle be determined by evaluating the initial

slope of the build-up curves, but the signal-to-noise ratio is usually not sufficient for short mixing times τ_m. It is preferable to estimate the initial slope by fitting the experimental build-up curve with the bi-exponential function of Equation 13, where the rates λ_1 and λ_2 are the eigenvalues of the system of two coupled equations of Equation 15. This only yields reasonable results if competing relaxation pathways are effectively quenched. To check just how effective this quenching needs to be, we analysed the effect of spin-diffusion on the build-up curves of $2N_zI_z$ and on the ratio r of Equation 12 through experiments and simulations.

To quench spin-diffusion among protons, two schemes were used. The scheme of Figure 3A was adapted from the QUIET-BIRD NOESY experiment (Zwahlen et al., 1994; Vincent et al., 1996). The use of two 180° pulses leads to the inversion of all longitudinal terms *except* N_z and $2N_zI_{lz}$. In this way the effect of cross relaxation between the neighbour and remote protons I_l and I_k on $2N_zI_{kz}$ terms is compensated to first order by a flow of opposite sign, thus partly quenching the effects of spin-diffusion. The scheme of Figure 3B, on the other hand, uses an off-resonance RF field on protons in order to quench cross-relaxation processes between all pairs of protons. If the correlation time is sufficiently long ($\tau_c \gg 1/\omega_I$), so that only $J_{lk}(0)$ contributes significantly in Equation 4, the weighted average of longitudinal and transverse cross-relaxation rates vanishes for $\theta_I = 35.3°$. In practice, two transients were added with offsets of opposite signs with respect to the center between the chemical shifts of neighbour and remote protons I_l and I_k (amide and H^α protons in the protein). This leads to a small average variation of the tilt angles (Desvaux and Goldman, 1996).

Figure 2 shows a typical two-dimensional spectrum of HiPIP, obtained with the sequence of Figure 1 with tilt angles $\theta_N = \theta_I = 35°$ and a mixing time $\tau_m = 70$ ms. Most residues can be identified, except for a few (such as His^{52}, Val^{68} and Tyr^{69}) that are too close to the paramagnetic Fe_4S_4 cluster to be observed.

Figure 4 shows the build-up curves obtained for three aminoacids (Glu^7, Tyr^{14} and Val^{60}) using two different schemes to quench spin diffusion, which are compared with experiments obtained without quenching spin diffusion. The relaxation rates (eigenvalues λ_1 and λ_2) resulting from fitting the build-up curves with the biexponential function of Equation 13 are reported in Table 1. A direct comparison of initial slopes is difficult. The QUIET scheme leads to an attenuation of the signals, mainly due to relaxation of transverse magnetization during the pulse sequence, but it does not affect the rates. On the other hand, off-resonance proton irradiation leads to a decrease of the cross-correlation rates (by a factor $1/\cos\theta_I$, which can be verified experimentally) and an increase of the self-relaxation rate of two-spin order. It is interesting to compare the experimental results with numerical simulations. In Figure 5, the decay of N_z and the build-up of $2N_zI_{lz}$ has been calculated using the complete relaxation matrix **R**. This may be compared to the behaviour that is predicted by considering only two coupled equations as in Equation 15. Clearly, spin-diffusion has little effect on the initial build-up, but a more pronounced effect at longer mixing times. This is described by the smallest eigenvalue λ_2 (longest time-constant), as may be appreciated in Figure 6. If the simulated build-up curves are fitted to Equation 13, it is the smallest eigenvalue λ_2 that is most affected by spin-diffusion. In a system with n spins, the curve decays slower for long mixing times than in a system with only two spins. If spin diffusion is active, the smallest eigenvalue λ_2 decreases and the longest time-constant becomes longer. Quenching spin-diffusion therefore appears to accelerate the decay. To simulate the quenching of spin diffusion by QUIET experiments, the signs of all terms except N_z and $2N_zI_{lz}$ were inverted in the middle of the mixing period. All terms except N_z were attenuated by an empirical coefficient 0.9 to account for losses due to transverse relaxation during the pulses sandwich. The build-up curve obtained in this way resembles that of a two-spin system. Figure 7 shows build-up curves for Leu^{59} and Ser^{73}, which have been chosen because they differ in the number of remote protons that occur in the vicinity of their amide protons.

Table 2 shows the ratio r, as defined in Equation 12, calculated for Leu^{59} and Ser^{73}. These ratios were derived from theoretical build-up curves computed with different methods for quenching proton-proton spin diffusion. When the proton magnetization is allowed to relax freely, the error of the ratio r is about 5% for Ser^{73} (low proton density) but rises to 10% for Leu^{59} (high proton density). With an ideal off-resonance irradiation with an effective field tilted at $\theta_I = 35.3°$ for all protons, all proton-proton cross-relaxation rates vanish. Not surprisingly, Table 2 shows that in this ideal case there are no errors in the determination of the ratio r of Equation 12, since the system is isolated from the surroundings. This proves

Table 1. (A) Relaxation rates (eigenvalues λ_1 and λ_2 in s^{-1}) obtained by fitting the experimental build-up curves of Figure 4 with the biexponential function of Equation 13 for three amino acids in HiPIP I. The self-relaxation rates $1/T_1(^{15}N)$ are also given. (B) Initial slopes (in arbitrary units) of the corresponding build-up curves

A

	without quenching		QUIET		$\theta_I = 35°$		inversion-recovery
	λ_1	λ_2	λ_1	λ_2	λ_1	λ_2	$1/T_1(^{15}N)$
Glu^{7}	15.9	0.51	7.6	1.8	20.1	1.1	2.17
Tyr^{14}	11.5	2.6	6.5	4.8	16.7	2.2	2.11
Val^{60}	22.9	1.4	9.8	3.4	22.1	1.8	2.16

B

	without quenching	QUIET	$\theta_I = 35°$
Glu^{7}	94.5	49.1	71.4
Tyr^{14}	81.9	58.2	78.4
Val^{60}	102.1	55.0	76.9

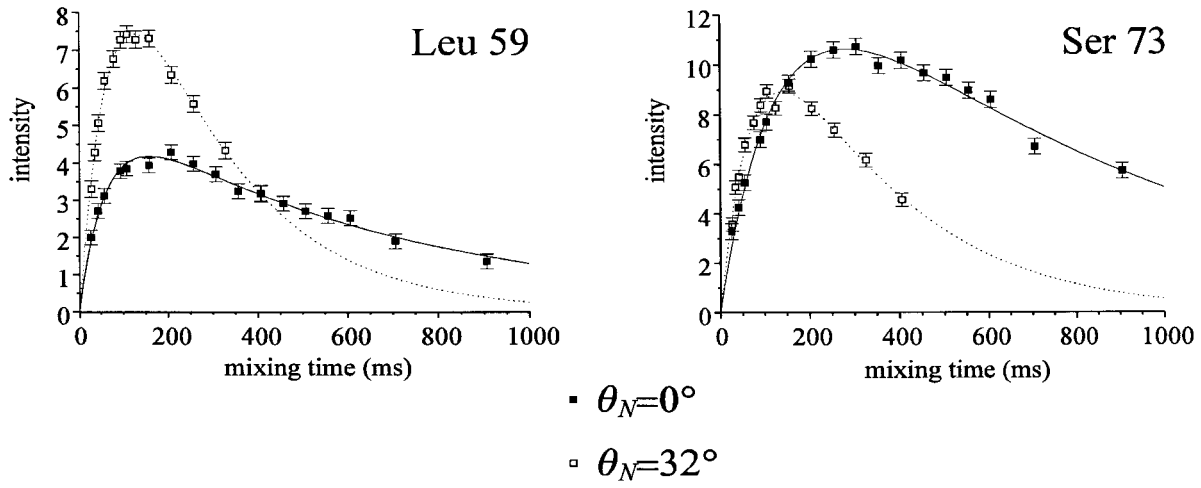

Figure 7. Build-up curves showing the conversion of N_z into $2N_zI_{lz}$, obtained with sequence of Figure 1, using $\theta_I = 35°$ to quench spin diffusion among the ^1H spins, and $\theta_N = 0°$ or 35° for the ^{15}N spins to estimate the ratio *r* of Equation 12. For Leu^{59} and Ser^{73}, the build-up curves were fitted to biexponential functions defined in Equation 13. In the rigid residue Leu^{59}, the fact that $J(0) > J(\omega_N)$ leads to a pronounced dependence on θ_N. In the highly mobile Ser^{73} residue, the initial slope of the build-up curve is almost independent of θ_N.

that relaxation pathways that are controlled by the rates σ^{NI} for both neighbour protons I_l and remote protons I_k and pathways that are determined by the rate $\delta^{N,NI}$ for remote protons I_k have little influence on the measurement of the rate $\delta^{N,NI}$ for neighbour protons I_l.

By contrast, the suppression of spin diffusion by the QUIET method does not depend on the spectral densities, but this approach can only be efficient if the rates are not much faster than the inverse of the mixing time (Schwager and Bodenhausen, 1996). In the simulations that have been summarized in Table 2, we have considered mixing times up to 1 s, while proton-proton cross-relaxation rates are on the order of several s^{-1}.

Finally, we have investigated the dependence of the measurements on the signal-to-noise ratio (see Figure 8.) We have simulated build-up curves with a proton irradiation with $\theta_I = 35.3°$and values of τ_m

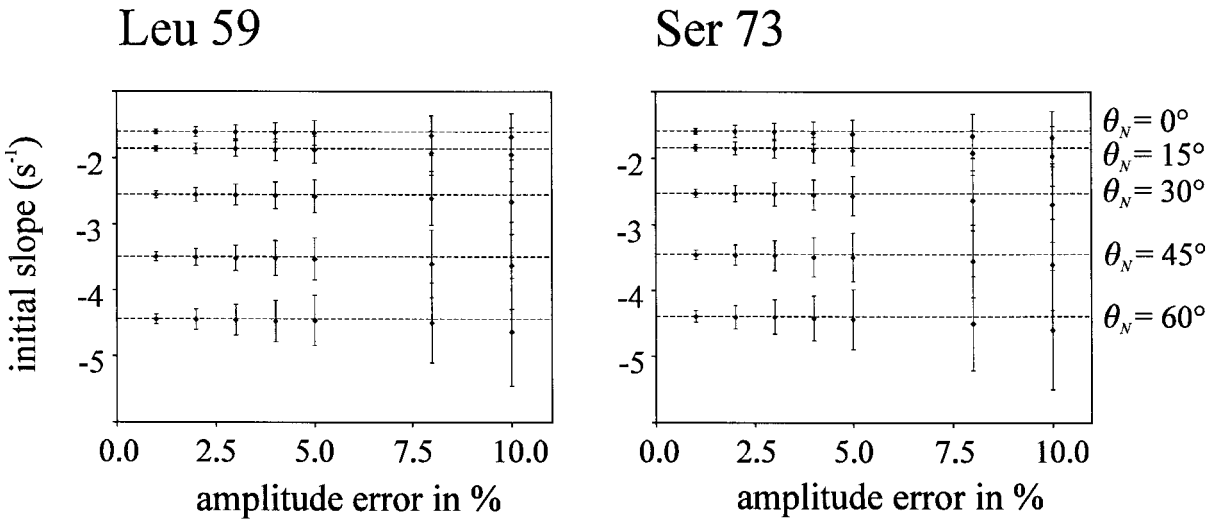

Figure 8. Effect on the estimates of initial slopes $\kappa^{N,NI}$ of errors added to cross-peak amplitudes. The points and error bars represent the averages and standard deviations obtained from 1000 runs where random errors were added to simulated build-up curves, considering 17 mixing times ranging between 25 and 900 ms. Five different tilt angles θ_N were considered while the proton tilt angle was kept constant to $\theta_I = 35°$. The parameters were those for Leu[59] and Ser[73] in HiPIP I. The horizontal dashed lines represent the exact values. A slight bias appears for large errors which lies well within the standard deviation.

that were close to the experimental values. By Monte-Carlo simulations, random errors were added to the simulated intensities. We have determined the average initial slopes $\langle \kappa_{fit}^{N,NI} \rangle$ and associated standard deviations. The average initial slopes are always larger than the exact ones. However, the differences between the average best-fit values and the exact values are smaller than the RMS deviations. The discrepancy between $\langle \kappa_{fit}^{N,NI} \rangle$ and $\kappa_{exact}^{N,NI}$ is largest for small angles θ_N and high proton density.

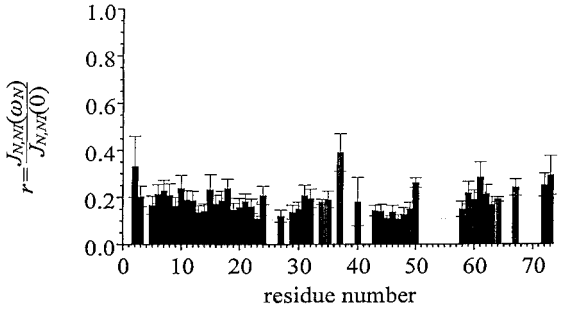

Figure 9. Ratios *r* as defined in Equation 12 for different amino-acid residues of HiPIP I.

Dynamic properties of the HiPIP I protein

Comparison of the initial slopes of the two buildup curves acquired with and without nitrogen irradiation gives an immediate measure of local mobility. Figure 7 shows experimental build-up curves for Leu[59], which lies in a rigid inner part of the protein, and for Ser[73], which is the last residue in the protein. When an off-resonance field is applied to the ^{15}N spins, the initial slope increases dramatically for Leu[59], but it is hardly affected for Ser[73]. This indicates that 'switching on' the effect of the spectral density contribution $J_{N,NI}(0)$ has a much larger effect for Leu[59] than for Ser[73]. This is a clear indication of the higher local mobility of Ser[73] compared to Leu[59].

The ratio *r* defined in Equation 12 has been determined for all observable amide groups in HiPIP I, as shown in Figure 9. Large values of *r*, indicating enhanced local mobility, can be observed for residues 3, 6, 7 , 8, 10, 15, 18, 24, 31, 40, 50, 59, 61, 62, 72, and 73. Several of these mobile residues (i.e., 6, 7, 8, 10, 15, 61, 62) are concentrated in a region packed around Tyr[14], as may be seen in Figure 10. This residue is conserved in all homologues of HiPIP from different photosynthetic bacteria, and its aromatic ring is close to the iron-sulfur cluster, thus contributing to a hydrophobic core around the cluster. Site-selective mutants of this residue with His, Trp, Ala, Leu, Phe, such as a Y14F mutation, were shown not to be very stable (Iwagami et al., 1995; Li et al., 1996). The Tyr[14] residue gives two hydrogen bonds, one as an acceptor with the side chain CO of Asn[16], one as a

Table 2. The dimensionless ratio *r*, as defined in Equation 12, extracted from numerical simulations of different schemes used to quench spin-diffusion. Errors in percent are given in brackets. Attention is focused on two amino acids with different proton densities: Ser^{73} has a lower density (12 remote protons within a sphere of 4.6 Å radius) and Leu^{59} has a higher density (12 remote protons within a sphere of 3.9 Å radius). The angle $\theta_I = 0°$ corresponds to free relaxation without irradiation on protons. For $\theta_I = 35.3°$, all cross-relaxation rates between protons vanish. The QUIET scheme of Figure 3B inverts all terms except N_z and $2N_z I_{lz}$ in the middle of the mixing period, which should cancel cross-relaxation processes among protons to first order

	Ser^{73} ($r_{exact} = 0.234$)			Leu^{59} ($r_{exact} = 0.232$)		
	$\theta_I = 0°$	$\theta_I = 35.3°$	QUIET	$\theta_I = 0°$	$\theta_I = 35.3°$	QUIET
$\theta_N = 15°$	0.253	0.234	0.256	0.235	0.232	0.237
	(+8.1%)	(0%)	(+9.4%)	(+1.3%)	(0%)	(+2.2%)
$\theta_N = 30°$	0.226	0.234	0.226	0.243	0.232	0.244
	(−3.4%)	(0%)	(−3.4%)	(+4.7%)	(0%)	(+5.2%)
$\theta_N = 45°$	0.227	0.234	0.228	0.257	0.232	0.258
	(−3%)	(0%)	(−2.6%)	(+10.8%)	(0%)	(+11.2%)
$\theta_N = 60°$	0.244	0.234	0.242	0.272	0.232	0.276
	(−4.3%)	(0%)	(+3.4%)	(+17.2%)	(0%)	(+19.0%)

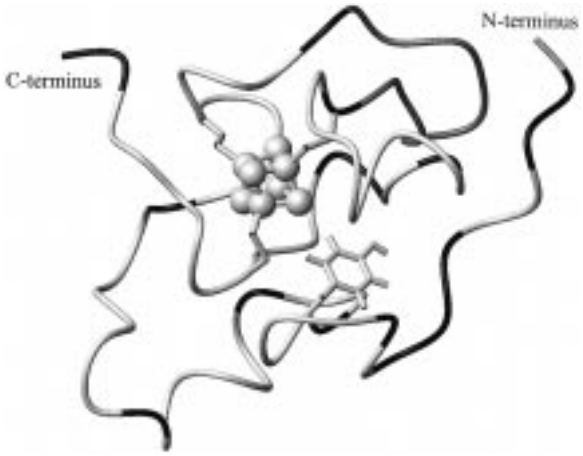

Figure 10. Ribbon diagram of the solution structure of HiPIP I from *E. halophila*. In addition to the backbone, the iron-sulfur cluster (large spheres) and the Tyr^{14} side chain are shown. Rigid residues with small *r* ratios as defined in Equation 12 are drawn in dark grey (upper right loop), partly mobile residues with medium *r* values are drawn in light grey, and highly mobile residues with high *r* values are drawn in black.

donor with the NH amide group of Lys^{61}, stabilizing a region of the protein involving residues 6, 7, 8, 10, 15, 61, and 62, where a higher internal mobility was detected. Another interesting region of the protein is the loop spanning residues 40–50, represented by a dark grey loop in the upper right of Figure 10. In this case, mainly low values of *r* are observed, with the exception of positions 40 and 50. This is quite surprising, since this region was found to crystallize in two different conformations (Breiter et al., 1991) and some discrepancies were observed between the calculated and the experimental proton NOEs (Bertini et al., 1996a). Therefore a high internal mobility was expected. Of course, this mobility could occur on a time scale that is slower than the overall correlation time of the protein, which cannot be detected by the methods described in this work. The residues around Phe^{38}, which separates the iron-sulfur cluster from the solvent molecule that is approximately opposite to Tyr^{14}, and which was suggested to be involved in the electron transfer, could not be detected. The NH group of this residue gives a hydrogen bond with a sulfur atom of the iron-sulfur cluster, like His^{52}, Cys^{66}, Val^{68}, Ala^{70}, for which build-up curves could not be recorded. Longitudinal ^1H self-relaxation rates for some of these protons were found to be very fast (e.g. $T_1 = 10$ ms for Val^{68}) (Bertini et al., 1996b). Therefore the self-relaxation rate of $2N_z I_{lz}$ must also be very fast, which should profoundly affect the shape of the build-up curve.

Conclusions

We have shown that information on the dynamics of N-H vectors can be obtained without using the self-relaxation rates $1/T_1\{^{15}N\}$ and $1/T_2\{^{15}N\}$ or $1/T_{1\rho}\{^{15}N\}$. The measurement of the cross-correlation

rate $\delta^{N,NI}$ can provide similar information. This approach is not affected by various relaxation mechanisms that contribute to the self-relaxation rates. Contributions from fast chemical exchange to transverse relaxation cannot interfere. This can be useful for both dia- and paramagnetic proteins. Therefore, this method, coupled to the measurement of $1/T_{1\rho}$ with variable spin-lock amplitude, provides a clean way to separate fast internal motions from motions that are slower than the overall rotational correlation time of the protein. The HiPIP I protein does not show a large dynamic heterogeneity. Only a region in the vicinity of Tyr^{14} shows a relatively high internal mobility. On the other hand, the region between residues 41–49 appears to be more rigid, although X-ray diffraction has indicated that this region may crystallize in different conformations.

Acknowledgements

This work was carried out with generous support of the National High Magnetic Field Laboratory, Tallahassee. Stimulating discussions with Dr Benoit Boulat, Dr Nagarajan Murali and Dr Pierre Mutzenhardt are gratefully acknowledged. We are greatly indebted to prof. Ivano Bertini for support and encouragement. Dr F. Capozzi and Dr M. S. Viezzoli gave precious suggestions for the expression and purification of the ^{15}N labeled protein sample.

References

Akke, M. and Palmer III, A.G. (1996) *J. Am. Chem. Soc.*, **118**, 911–912.

Banci, L., Bertini, I. and Luchinat, C. (1991) *Nuclear and Electron Relaxation*, VCH, Weinheim.

Banci, L., Bertini, I., Eltis, L.D., Felli, I.C., Kastrau, D.H.W., Luchinat, C., Piccioli, M., Pierattelli, R. and Smith, M. (1994) *Eur. J. Biochem.*, **225**, 715–725.

Bax, A., Ikura, M., Kay, L.E., Torchia, D.A. and Tschudin, R. (1990) *J. Magn. Reson.*, **86**, 304–318.

Bertini, I., Luchinat, C. and Tarchi, D. (1993) *Chem. Phys. Lett.*, **203**, 445–449.

Bertini, I., Felli, I.C., Kastrau, D.H.W., Luchinat, C., Piccioli, M. and Viezzoli, M.S. (1994) *Eur. J. Biochem.*, **225**, 703–714.

Bertini, I., Felli, I.C., Luchinat, C. and Rosato, A. (1996a) *Proteins Struct. Funct. Genet.*, **24**, 158–164.

Bertini, I., Couture, M.M.J., Donaire, A., Eltis, L.D., Felli, I.C., Luchinat, C., Piccioli, M. and Rosato, A. (1996b) *Eur. J. Biochem.*, **241**, 440–452.

Bertini, I. and Luchinat, C. (1996c) *NMR of paramagnetic substances, Coordination Chemistry Reviews*, Elsevier, Amsterdam.

Boelens, R., Koning, T.M.G. and Kaptein, R. (1988) *J. Mol. Struct.*, **173**, 299–311.

Borgias, B.A., Gochin, M., Kerwood, D.J. and James, T.L. (1990) *Prog. NMR Spectrosc.*, **22**, 83–100.

Boyd, J., Hommel, U. and Campbell, I. (1990) *Chem. Phys. Lett.*, **175**, 477–482.

Brüschweiler, R. and Ernst, R.R. (1991) *J. Chem. Phys.*, **96**, 1758–1766.

Breiter, D.R., Meyer, T.E., Rayment, I. and Holden, H.M. (1991) *J. Biol. Chem.*, **266**, 18660–18667.

Dayie, K.T. and Wagner, G. (1994) *J. Magn. Reson.*, **A111**, 121–126.

Cordier, F., Brütscher, B. and Marion, D. (1996) *J. Biomol. NMR*, **7**, 163–168

Desvaux, H., Berthault, P., Birlirakis, N., Goldman, M. and Piotto, M. (1995) *J. Magn. Reson.*, **A113**, 47–52.

Desvaux, H. and Goldman, M. (1996) *J. Magn. Reson.*, **B110**, 198–201.

Desvaux, H. (1997) *J. Magn. Reson.*, **127**, 1–16.

Dickson, D.P.E., Johnson, C.E., Cammak, R., Evans, M.C.W., Hall, D.O. and Rao, K. (1974) *Biochem. J.*, **139**, 105–108.

Ernst, R.R., Bodenhausen, G. and Wokaun, A. (1987) *Principles of Nuclear Magnetic Resonance in One and Two Dimensions*, Clarendon Press, Oxford.

Farrow, N.A., Muhandiram, R., Singer, A.U., Pascal, S.M., Kay, C.M., Gish, G., Shoelson, S.E., Pawson, T., Forman-Kay, J.D. and Kay, L.E. (1994) *Biochemistry*, **33**, 5984–6003.

Grzesiek, S. and Bax, A. (1993) *J. Am. Chem. Soc.*, **115**, 12593–12594.

Guéron, M. (1975) *J. Magn. Reson.*, **19**, 58–66.

Iwagami, S.G., Creagh, A.L., Haynes, C.A., Borsari, M., Felli, I.C., Piccioli, M. and Eltis, L.E. (1995) *Protein Sci.*, **4**, 2562–2572.

Kay, L.E., Torchia, D.A. and Bax, A. (1989) *Biochemistry*, **28**, 8972–8979.

Kay, L.E., Nicholson, L.K., Delaglio, F., Bax, A. and Torchia, D.A. (1992) *J. Magn. Reson.*, **97**, 359–375.

Lefèvre, J.F., Dayie, K.T., Peng, J.W. and Wagner, G. (1996) *Biochemistry*, **35**, 2674–2686.

Li, D., Agarwal, A. and Cowan, J.A. (1996) *Inorg. Chem.*, **35**, 1121–1125.

Lipari, G. and Szabo, A. (1982) *J. Am. Chem. Soc.*, **104**, 4546–4559.

Mäler, L., Mulder, F.A.A. and Kowalewski, J. (1996) *J. Magn. Reson.*, **A117**, 220–227.

Malliavin, T.E., Delsuc, M.-A. and Lallemand, J.Y. (1992) *J. Biomol. NMR*, **2**, 349–360.

Palmer III, A.G., Skelton, N.J., Chazin, W.J., Wright P.E. and Rance, M. (1992) *Mol. Phys.*, **75**, 699–711.

Palmer III, A.G., Williams, J. and McDermott, A. (1996) *J. Phys. Chem.*, **100**, 13293–13310.

Peng, J.W. and Wagner, G. (1992) *J. Magn. Reson.*, **98**, 308–332.

Peng, J.W. and Wagner, G. (1995) *Biochemistry*, **34**, 16733–16752.

Pervushin, K., Riek, R., Wider, G. and Wüthrich, K. (1997) *Proc. Natl. Acad. Sci. USA*, **94**, 12366–12371.

Piotto, M., Saudek, V. and Sklenar, V. (1992) *J. Biomol. NMR*, **2**, 661–665.

Press, W.H., Flannery, B.P., Teukolsky, S.A. and Vetterling, W.T. (1992) *Numerical recipes in C*, 2nd ed., Cambridge University Press, Cambridge.

Reif, B., Hennig, M. and Griesinger, C. (1997) *Science*, **276**, 1230–1233.

Sklenar, V., Torchia, D. and Bax, A. (1987) *J. Magn. Reson.*, **79**, 375–379.

Schwager M. and Bodenhausen, G. (1996) *J. Magn. Reson.*, **B111** 40–49.

Solomon, I. (1955) *Phys. Rev.*, **99**, 559–565.

Tjandra, N., Szabo, A. and Bax, A. (1996a) *J. Am. Chem. Soc.*, **118**, 6986–6991.
Tjandra, N., Wingfield, P., Stahl, S. and Bax, A. (1996b) *J. Biomol. NMR*, **8**, 273–284.
Vasavada, K.S. and Nageswara Rao, B.D. (1989) *J. Magn. Reson.*, **81**, 275–283.
Vincent, S.J.F., Zwahlen, C., Bolton, P.H., Logan, T.M. and Bodenhausen, G. (1996) *J. Am. Chem. Soc.*, **118**, 3531–3532.
Wagner, G. (1993) *Curr. Opin. Struct. Biol.*, **3**, 748–754.
Werbelow, L. and Thévand, A. (1993) *J. Magn. Reson.*, **101**, 317.
Zeng, L., Fischer, M.W.F. and Zuiderweg, E.R.P. (1996) *J. Biomol. NMR*, **7**, 157–162.
Zinn-Justin, S., Berthault, P., Guenneuges, M. and Desvaux, H. (1997) *J. Biomol. NMR*, **10**, 363–372.
Zwahlen, C., Vincent, S.J.F., Di Bari, L., Levitt, M.H. and Bodenhausen, G. (1994) *J. Am. Chem. Soc.*, **116**, 362–368.